Thermal transport properties of penta-graphene with grain boundaries

Jie Sun [a], Yaguang Guo [a, b], Qian Wang [a, *], Yoshiyuki Kawazoe [c]

[a] Center for Applied Physics and Technology, Department of Materials Science and Engineering, HEDPS, College of Engineering, Peking University, Beijing, 100871, China
[b] Department of Biomedical Engineering, College of Engineering, Peking University, Beijing, 100871, China
[c] New Industry Creation Hatchery Center, Tohoku University, Sendai, 980-8577, Japan

ARTICLE INFO

ABSTRACT

Penta-graphene (PG), composed of carbon pentagons, has attracted considerable attention because of its unique atomic configuration and novel properties. Here, for the first time, we study the effect of grain boundaries (GBs) on the thermal transport properties of PG by using non-equilibrium molecular dynamics simulations. Compared with pristine PG, the thermal conductivity of grains in polycrystalline penta-graphenes (PPGs) decreases by about 20%. The boundary conductance of PPGs with different GBs is in a small range of 0.43×10^{10} to 0.57×10^{10} W/mK, which differs from the situation of polycrystalline graphene where the boundary conductance decreases dramatically with the increase of grain orientation angles. The critical size of the grains is found to be about 25 nm, below which the contribution from GBs to the thermal conductivity is comparable to that from the grains. This critical size is much smaller than that of polycrystalline graphene (100 nm). A detailed analysis of the phonon group velocity and vibrational density of states reveals that the geometric anisotropy and the phonon scattering induced by the GBs in PPG are the main reasons for the reduction of thermal conductivity. Our study sheds lights on tuning thermal conductivity via GB engineering in 2D materials.

© 2019 Published by Elsevier Ltd.

1. Introduction

We recently proposed a two dimensional (2D) carbon allotrope, penta-graphene (PG) [1], composed entirely of carbon pentagons, which is structurally related to the previously studied T12-carbon [2]. Its geometric structure resembles a famous 2D pattern named Cairo pentagon tiling, and its thermodynamic stability is over the experimentally synthesized dodecahedral C_{20} [3], implying that PG could be realized experimentally. PG has received tremendous attention because of its exotic atomic configuration and intriguing properties [4—36]. Based on the geometric structure of PG, other pure pentagon-based 2D materials including penta-SiC_2 [14—16], penta-B_2C [17], penta-PdS_2 [18], penta-CN_2 [19], penta-silicene [20], penta-ZnO_2 [21], penta-SnX_2 (X = S, Se, or Te) [22], and penta-AlN_2 [23], have been theoretically proposed or experimentally synthesized [24]. Further studies on the properties of PG have also been carried out [7,9,16,26—31]. For example, Quijano-Briones

et al. studied the structural and electronic properties of PG nanotubes and doped PG [34,35]. Liu et al. investigated the electronic and magnetic properties of PG when introduced a hydrogen atom [36]. Besides, stimulated by the fantastic thermal transport properties of carbon allotropes, the thermal conductivity is particularly of interest and has been widely studied [16,28—30,32,33]. For instance, the room temperature lattice thermal conductivity of amorphous carbon is about 0.01 W m^{-1} K^{-1} [37] while the value for graphene is in the range of 3000—5800 W m^{-1} K^{-1} [38—41]. The thermal conductivity of PG was found to be 167 W/mK by using classical equilibrium molecular dynamics simulations [32], which is much lower than that of graphene. To further tune the thermal conductivity of PG, several approaches have been proposed. For example, Liu et al. [16] studied the effect of external tensile strength on the thermal conductivity of PG, and found that the thermal conductivity of PG decreases monotonically by stretching. Wu et al. [29] found that, in contrast to graphene, hydrogenation of PG can significantly increase the thermal conductivity, which results from the weaker anharmonicity of the C-C bonds.

In addition to strain effect and surface modulation, it has been demonstrated that introducing line defects is also an effective way

---

to tune the thermal transport properties of materials [42—45]. The most common line defect is grain boundary (GB) in polycrystals and its influence can be quantified by Kapitza conductance (boundary conductance) [46,47]. For graphene, Hahn et al. [48] found that the nanograins with a radius of gyration of 1 nm leads to a reduction of the thermal conductivity of 3%, because of the decrease of vibrational state with high density induced by GBs. Ma et al. [49] showed that the thermal conductivity of graphene sheet dramatically decreases with decreasing grain size by a small thermal boundary conductance of 3.8×10^9 W/m²K. Theoretically, it was found that the contribution of GBs to thermal conductivity becomes comparable to that from grains when grain size is below 0.1 μm [50]. These findings imply that GBs play an important role in tuning the thermal transport properties of graphene. However, to our best knowledge, there are no studies reported so far on the effect of GBs on thermal transport properties of PG, which motivates us to conduct this research.

In this paper, we systematically study the effect of GBs on the thermal transport properties of PG and focus on the two questions: (1) What are the stable geometric configurations of GBs in PG? (2) What is the effect of GBs on the thermal transport properties of PG? To answer the questions, we first determine the stable GB models of PG, and then we calculate the thermal transport properties of the polycrystalline PGs (PPGs) with different grain orientations. We find that the boundary conductance is largely dependent on the defect density (number of non-pentagon rings) in the GB region, and the geometric anisotropy and grain size play important roles in determining the thermal conductivity of polycrystalline PG.

2. Computational methods

We use the reverse non-equilibrium molecular dynamics (RNEMD) method [51] to calculate the thermal conductivity. The main idea of this method is to develop a heat flux through the structure and obtain temperature gradient along the heat flux direction. By transferring energy from a "cold" slab, located at the ends of simulation model, to a "hot" slab, located at the middle of simulation model, the heat flux is imposed in the model. This is realized by exchanging the velocities of the hottest atom in the cold slab with the coldest atom in the hot slab, as is shown in Fig. 1. The heat flux introduced in this model is described as

$$q = \frac{1}{2tA_{yz}} \sum \frac{m}{2} \left(v_{hot}^2 - v_{cold}^2 \right) \tag{1}$$

where q is heat flux, t is the time of energy transferring, A_{yz} is the cross-sectional area perpendicular to the hot flow direction, defined as $A_{yz} = wd$, (w and d are the width and thickness of the sheet, respectively). The interlayer distance of graphite (3.35 Å), is chosen as the thickness when dealing with graphene [52]. Wu et al.

choose this value as the thickness of PG to study their thermal conductivity to make a comparison with other 2D materials [29]. The thickness of PG can also be defined as the sum the structural buckling height and two van der Waals radius of carbon atoms (4.8 Å) [32]. In our study, we choose the former one to calculate the thermal transport properties of PG with grain boundaries, which can eliminate the effect of thickness when comparing with the corresponding properties of graphene. v_{hot} and v_{cold} are the velocities of the hottest and coldest atoms in the cold and hot regions, respectively. The factor 2 represents the two directions of heat flux. Based on Fourier's law, the thermal conductivity can be derived from the heat flux as

$$k = \frac{q}{\partial T / \partial x} \tag{2}$$

where k is thermal conductivity, $\partial T / \partial x$ is temperature gradient along the heat transport direction.

In addition to the phonon-phonon scattering happened in the sample, phonon scattering also exists at the heat baths or boundaries, when a heat flux travels through the structure. The latter becomes dominant when sample size is smaller than the phonon mean free path (MFP) [53,54]. In this scenario, the thermal conductivity depends on the sample length. The two phonon scattering mechanisms lead to the size effect of thermal conductivity. The thermal conductivity and sample length L satisfy the relation

$$\frac{1}{k} = \frac{1}{k_\infty} \left(\frac{l_{ph-ph}}{L} + 1 \right) \tag{3}$$

where k_∞ is the thermal conductivity of the sample with an infinite length and l_{ph-ph} is the effective phonon mean free path. As implied by Eq. (3), a plot of the inverse of thermal conductivity versus the size of sample length should be a linear curve.

The Kapitza conductance G, namely boundary conductance, is defined as the ratio of heat flux q to the temperature jump ΔT [47]:

$$G = \frac{q}{\Delta T} \tag{4}$$

The RNEMD simulations are carried out by using the large-scale atomic/molecular massively parallel simulation (LAMMPS) molecular dynamics package. For potential, Szymon et al. [55] tested the interatomic potentials for PG and found that Tersoff-type potential proposed by Erhart and Albe [56] in 2005 can reasonably describe the structural, mechanical and energetic parameters of PG. While Wen et al. [32] found that the original Tersoff potential can not only describe the structural and mechanical properties of PG, but also gives a well reproduction of unusual Poisson's ratio and phonon dispersion within 25 THz. We have calculated the length of C-C bonds in PG with Tersoff potential. The bond length between sp^3 and sp^2 C atoms is 1.55 Å, while the value for two sp^2 C atoms is
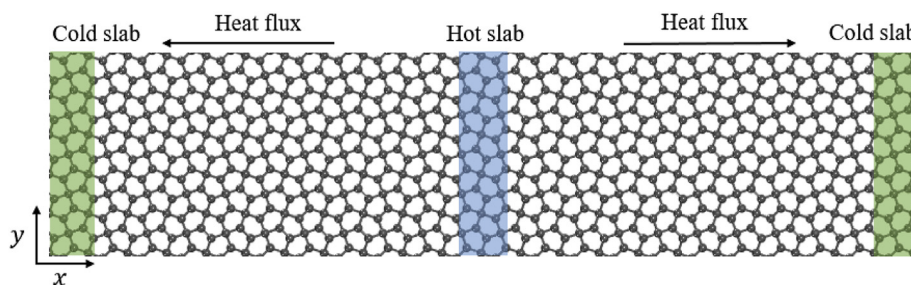

Fig. 1. The model used in RNEMD simulation. The hot and cold slabs are located at the middle and ends of the supercell, respectively. (A colour version of this figure can be viewed online.)

1.48 Å (see Fig. S1). These results are consistent with those of DFT calculations, which verifies the validity of choosing Tersoff potential for PG [1]. Therefore, in this study, we choose the original Tersoff potential for calculations.

The simulation time step is set to 0.5 femtosecond (*fs*) and periodic boundary condition is applied to all the three directions. The structures are first thermalized in NVT ensemble at room temperature for 1×10^6 steps, and then run in NVE ensemble for another 1×10^6 steps until the forces on atoms are less than 10^{-8} eV/Å. The atoms in hot and cold regions are exchanged every 100 time steps. Structures are allowed to evolve for 5×10^5 time steps to obtain a steady temperature profile. Then, the temperature gradient is obtained after over 9.5×10^6 time steps. Every structure is divided into 50 slabs.

3. Results and discussion

Unlike the well-established GB structures in graphene [50,57–60], there is no study reported so far on GB structures in PG. Therefore, we first need to find the stable GB structures. Six GB structure models with the orientation angles ranging from 16.26° to 53.13° are generated based on CSL theory [61], choosing the *y* axis as the GB edge and the *z* axis as the rotation axis, where the two grains are rotated by a small angle until their surface planes coincide with each other. For a given misorientation angle, there are several possible geometric configurations. The stable GB structures can be identified through structural optimization of different initial structures. More details can be found in section S2 and S3 of Supplementary Material. Since these constructed GB models are generally under strain due to the unsaturated bonds in the GB regions, we optimize the six geometries, and calculate their GB energies E_{GB}, which is defined as $E_{GB} = (E_{PPG} - E_{PG})/4l$, where E_{PPG} and E_{PG} are the total energies of PG with and without GBs, respectively, and *l* is the length of the GB edge. The factor of 4 accounts for the existence of four equivalent GBs in the supercell. The calculated results are given in Fig. 2. The three structures of PPGs with GB orientation angles of 16.26°, 22.61°, and 31.89° are plotted in Fig. 3. The length of *l* is the periodic length along the direction, as shown in Fig. S4. One can see that the structures with GB orientation angles of 16.26°, 22.61°, and 31.89° have smaller E_{GB} as compared to that of others. Therefore, we choose the three low-laying energy structures of PPG for further investigation. We note that the GB regions in PPG are composed of 4-, 5-, 6-, and 7-rings, which are less regular than those of graphene [50], leading to complicated behaviors of energy changes with the angle. For example, when going from 16.26° to 22.61° and 31.89°, the 5-member ring density (the ratio of the number of pentagons to the total number of the rings) increases from 0.17 to 0.33 and 0.40, and the total non-5-member ring density decreases from 0.83 to 0.67 and 0.60, while the GB energy oscillates as shown in Fig. 2, suggesting that there is no simple relationship between GB energy and the type of defect.

To validate our computational method, we first calculate the thermal conductivity of pristine PG. The temperature distribution along the length direction is plotted in Fig. 4(a), which exhibits linear patterns away from the hot and cold ends, as indicated in orange lines. The nonlinear parts are caused by the edge effects, while only the linear portions are considered when calculating the temperature gradient. We find that the calculated thermal conductivity of PG depends on the size of the model, and the values are 32.34, 52.94, and 68.36 W/mK for the length of 25, 50, and 75 nm, respectively. The variation of the inverse of thermal conductivity with the inverse of grain size for PG is plotted in Fig. 5(a). We then extract the thermal conductivity by extrapolating the linearly fitted curve (red dotted line in Fig. 5(a)), and find that k_{PG} is 151.52 W/mK from the intercept. This value is in good agreement with the previous MD result (167 W/mK) [29], confirming the reliability of the method used in our work. The small difference is attributed to the different thicknesses and ensembles applied during the simulations. The thermal conductivity of PG when choosing the thickness of 4.8 Å is discussed in section S5 of Supplementary Material.

Next, we study the thermal transport properties of PPGs with the three different orientation angles. In previous study, the total length of polycrystalline graphene is set as 25 nm, 50 nm, and 75 nm [50]. For convenience of comparison, we choose these values to perform our MD simulations for PG, which can eliminate the size effect in calculating thermal conductivity. Because the four GBs are equivalent, the length of two neighbouring blue area is a quarter of the total length. Since we use NPT ensemble to fully relax the structure, the internal stress is released during the optimization. Therefore, the length has little effect on the stress inside the PPGs. We note that the major difference between temperature profiles of pristine and PPGs, as shown in Fig. 4(a) and (b), respectively, is the existence of the sharp jumps at each position of grain boundaries for the system with the orientation angle of 22.61°. The jumps separate the linear parts of temperature profile from the two neighbouring grains. We then calculate the thermal conductivity of the grains with different orientation angles. The variation of the inverse of thermal conductivity with inverse of system size (box length) is plotted in Fig. 5(a). One can see, similar to pristine PG, that the inverse of thermal conductivity of the oriented grains has an almost linear relationship with the inverse of system size. The calculated thermal conductivities are 120.48, 112.36 and 128.20 W/mK for the grains with orientation angles of 16.26°, 22.61°, and 31.89°, respectively. We note that the thermal conductivity of the grains decreases by about 20% as compared to that of pristine PG (151.52 W/mK). There are two possible reasons accounting for the reduction. One is the increase of additional phonon scattering in the GB regions, leading to a decrease of the thermal conductivity. The other is the geometric anisotropy that reduces the thermal conductivity, because the directions are non-equivalent in the PPGs due to the square 2D lattice of PG. To further understand it, we take the 22.61° grain as an example and study the thermal conductivity of this defect-free structure with a certain orientation angle (rotated PG) to avoid the effect of the phonon scattering at GB. Fig. 5(b) shows the relationship between the thermal conductivity and sample size, where we obtain the thermal conductivity of PG with 22.61° orientation by extracting the intercept (128.21 W/mK). In this case, the thermal conductivity also decreases by nearly 15%, indicating that the anisotropic effect of PG is a key factor to determine its thermal conductivity. Compared with the value of 112.36 W/mK, one can see a difference of the calculated thermal
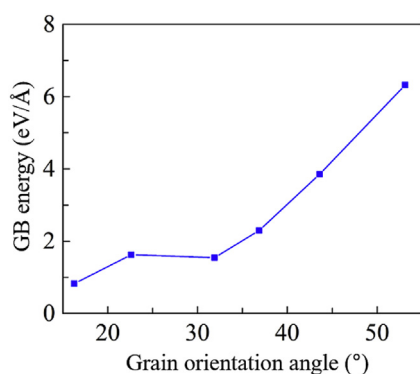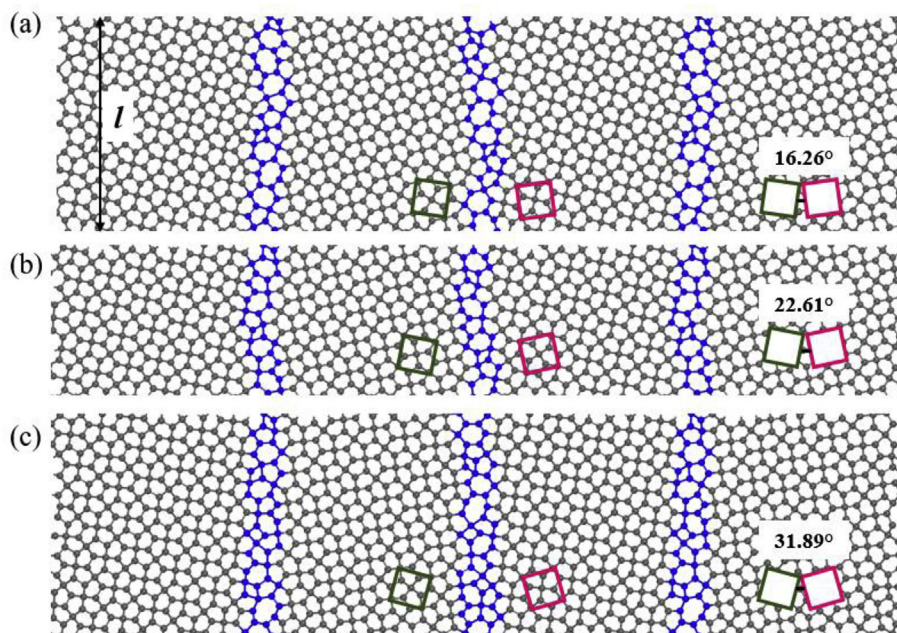

Fig. 2. Calculated GB energies with the different orientation angles. (A colour version of this figure can be viewed online.)

Fig. 3. Structure of PPG with the grain orientation angle of (a) 16.26°, (b) 22.61°, and (c) 31.89°. The angles between the green and pink squares represent the GB orientation angles between the two neighbouring grains. (A colour version of this figure can be viewed online.)
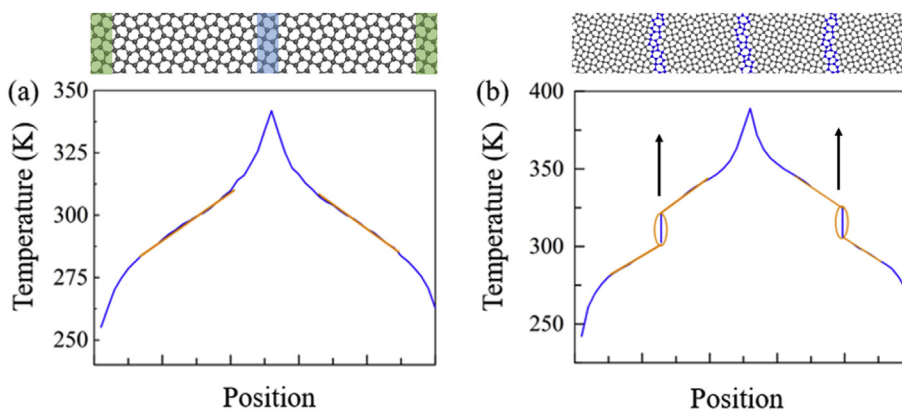
Fig. 4. Temperature profile along the length direction of (a) pristine PG, and (b) PPG with grain orientation angle of 22.61°. (A colour version of this figure can be viewed online.)
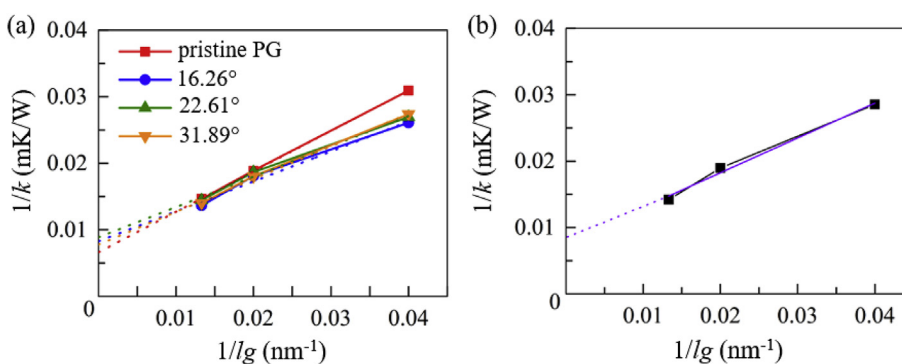
Fig. 5. (a) Inverse of the thermal conductivities of pristine PG and PPGs versus the inverse of the simulation box length (lg). (b) Inverse of the thermal conductivity of rotated PG (22.61°) versus the inverse of box length (lg). (A colour version of this figure can be viewed online.)

conductivity between the two models. This can be solely attributed to the phonon scattering in the GB regions. Anisotropic effect is rarely considered when calculating the thermal conductivity of 2D materials with non-hexagonal symmetry. The thermal transport direction in previous works is usually parallel to the crystal axis [16,28,29,32], which omits the influence of incident heat flux direction. Therefore, the above results demonstrate that the thermal conductivity depends on the orientation of the 2D sheet, suggesting that the geometric anisotropy cannot be neglected in simulations.

To further explore the mechanism of the reduction of thermal conductivity, the phonon group velocity of pristine PG and rotated PG with grain orientation angle of 22.61° are calculated by using PHONOPY [62]. The calculated results are plotted in Fig. 6 (a). One can see that in the whole frequency region, the phonon group velocity of pristine PG is larger than that of rotated PG. The phonon group velocity of rotated PG in the middle and high frequency region (10—50 THz) is smaller than 5000 m/s and most of the phonon group velocity is smaller than 10000 m/s in low frequency region (0-10 THz), while that for pristine PG is larger than 10000 m/s in the low frequency region (0—10 THz). The reduced phonon group velocity of rotated PG leads to the reduction in thermal conductivity.

We then calculate the vibrational density of states (VDOS), which can describe the distribution of phonons with different frequencies, by taking a Fourier transform on the atom velocity autocorrelation function [63,64]. Fig. 6 (c) and (d) show the VDOS of the two regions (see Fig. 6. (b)) in pristine PG and PPG (22.61°), respectively. The VDOS of the two regions are almost overlapped in pristine PG. While for the PPG, the deviation between the VDOS of two regions is noticeable. In the frequency range of 40—45 THz, the peak of VDOS for region 1 has a deviation from that for region 2.

Similar deviation also shows in the frequency range of 5—10, 20—25, 30—35 THz. The overlap between two VDOS can be quantified by integrating the spectra over frequency,

$$I = \int f_1(\omega) f_2(\omega) d\omega \tag{5}$$

where $f_1(\omega)$ and $f_2(\omega)$ is the spectral function of phonon mode frequency ω of two regions. Based on Eq. (5), the overlap of pristine PG and the PPG are calculated to be 0.23 and 0.15, respectively, showing that the overlap of PPG is smaller than that of pristine PG, resulting more vibrational mismatch. Such vibrational mismatch will decrease the heat transfer efficiency in the structure, thus leading to the decrease in thermal conductivity.

We then study the thermal transport in the GB regions by calculating the boundary conductance. Table 1 shows a summary of the temperature jumps and the heat flux for the PPGs with the different grain sizes and grain orientations, from which boundary conductance can be calculated based on Eq. (4). We find that the values of boundary conductance are in a small range from 0.43×10^{10} to 0.57×10^{10} W/m²K. These values are in one order of magnitude smaller than that of polycrystalline graphene calculated by Akbar et al. [50], but two or three times larger than that of ultrananocrystalline diamond thin films with GBs [65], Si-Ge interface and Si-Si (001) Σ29 GBs, respectively [66,67]. We note that the boundary conductance of PPG depends weakly on the grain orientation angles. This is different from that of polycrystalline graphene, where the boundary conductance decreases with the increase of the grain orientation angle [50]. A rational understanding is, in polycrystalline graphene, the increase of defect
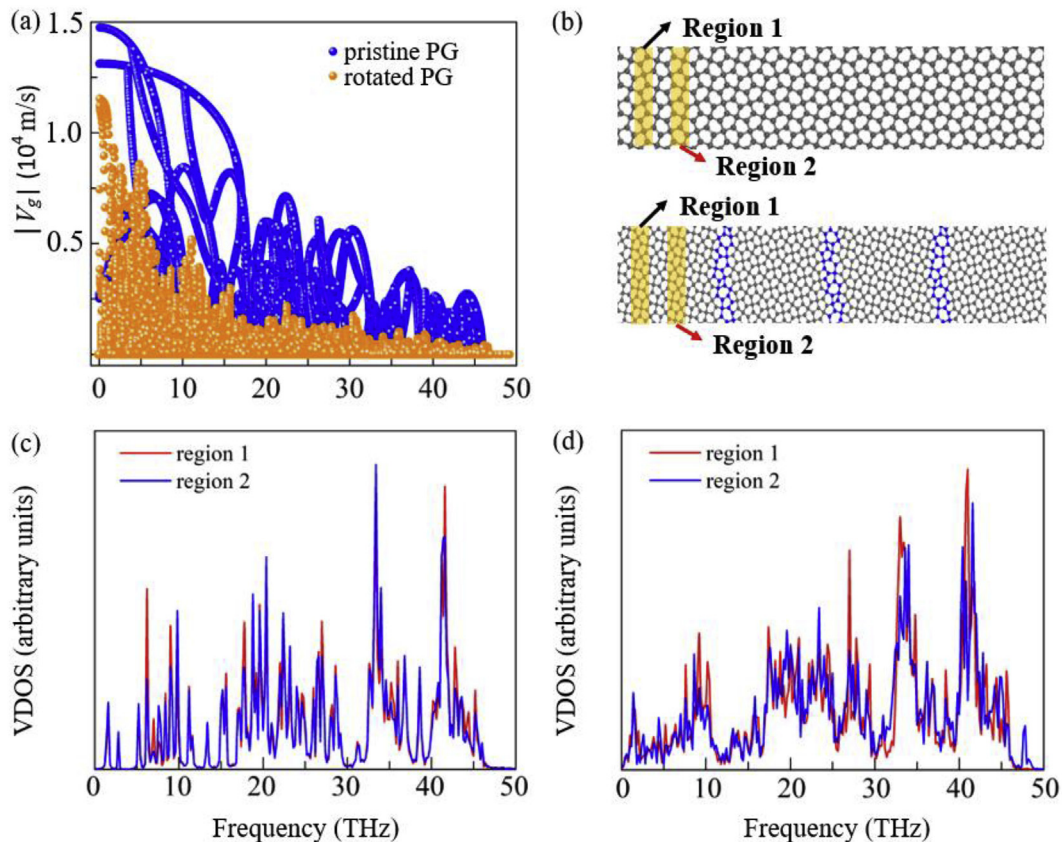
Fig. 6. (a) Absolute value of the phonon group velocities (V_g) of pristine PG and the rotated PG (22.61°), (b) Schematic diagram of pristine PG and PPG (22.61°) with two regions, (c) and (d) Vibrational density of states of pristine PG and PPG, respectively. (A colour version of this figure can be viewed online.)

Table 1
Temperature jumps (in K) and heat flux (in W/m^2), given in brackets, for the PPGs with different grain sizes and orientation angles.

Grain orientation angle	25 nm grain size	50 nm grain size	75 nm grain size
16.26°	44.61 (1.95×10^{11})	45.51 (1.98×10^{11})	42.16 (1.97×10^{11})
22.61°	45.61 (2.53×10^{11})	45.40 (2.57×10^{11})	51.95 (2.53×10^{11})
31.89°	47.86 (2.24×10^{11})	54.92 (2.23×10^{11})	49.35 (2.18×10^{11})

density as the grain orientation angles becomes larger, thus leading to a drop in the boundary conductance caused by more phonon scattering. On the contrary, the defect density in PPG does not exhibit an obvious correlation with the grain orientation angles, so that phonon scattering changes little at different GB regions. Note that the calculated conductance also slightly depends on the size of grains (see Fig. 7), which is similar to the cases of GBs in graphene [50], Si-Ge and silicon [68], where scattering of long wavelength phonons at heat reservoirs and at the boundaries exist.
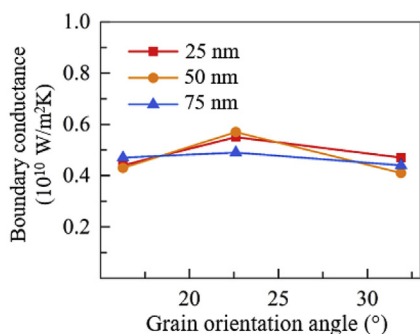
As the grain size increases, the effect of GBs on thermal conductivity becomes weaker, where the phonon scattering is primarily decided by the grain itself instead of the GBs. However, when the grain size decreases, the contribution from GBs to the thermal conductivity becomes more dominant. For the PPG, the thermal conductivity k_p can be written as

$$k_p^{-1} = k_g^{-1} + \left(G l_g \right)^{-1} \tag{6}$$

where k_g is the thermal conductivity of grain, l_g is the grain spacing. By using this expression together with the calculated boundary conductance, we estimate the critical size of the grains, below which the contribution from GBs are comparable to that of the scattering from the grains. The length scale is simply the ratio of thermal conductivity to the boundary conductance. For our studied system, the length scale is of the order of 25 nm, which is much smaller than that of polycrystalline graphene (0.1 μm) [50]. This finding clearly indicates that in large scale synthesis of PG, no special attentions or skills are needed to control the grain boundaries for reducing the effect on thermal conductivity.

4. Conclusions

In this work, the effect of grain boundaries on the thermal transport properties of PG has been systematically studied for the first time by using RNEMD simulations. Based on the CSL theory, we have constructed six GB structure models, and selected three low-lying energy configurations with orientation angles of respectively 11.26°, 22.61°, and 31.89° for further investigation, and their corresponding thermal conductivities are calculated to be 120.48, 112.36 and 128.20 W/mK at room temperature, respectively, which

are decreased by about 20% as compared to that of pristine PG. The boundary conductance of PPGs with the different orientation angles changes in a narrow range of 0.43×10^{10} to 0.57×10^{10} W/mK. In addition, we have further identified the main factors affecting the thermal conductivity: (1) phonon scattering caused by the existence of GBs; (2) the reduced phonon group velocity; (3) the mismatch of vibrational density of states in PPGs resulted from the geometric anisotropy of PPG. These findings would help us to comprehend the thermal conductivity of 2D carbon materials beyond the well-studied graphene.

Appendix A. Supplementary data

Supplementary data to this article can be found online at https://doi.org/10.1016/j.carbon.2019.01.015.

Fig. 7. Boundary conductance of GBs in PPG with different orientation angles. (A colour version of this figure can be viewed online.)

References

[1] S. Zhang, J. Zhou, Q. Wang, X. Chen, Y. Kawazoe, P. Jena, Penta-graphene: a new carbon allotrope, Proc. Natl. Acad. Sci. Unit. States Am. 112 (2015) 2372–2377.

[2] Z. Zhao, F. Tian, X. Dong, Q. Li, Q. Wang, H. Wang, X. Zhong, B. Xu, D. Yu, J. He, Tetragonal allotrope of group 14 elements, J. Am. Chem. Soc. 134 (30) (2012) 12362–12365.

[3] S. Fischer, P.C. Weber, Thromboxane A3 (TXA3) is formed in human platelets after dietary eicosapentaenoic acid (C20: 5ω3), Biochem. Biophys. Res. Commun. 116 (3) (1983) 1091–1099.

[4] B. Rajbanshi, S. Sarkar, B. Mandal, P. Sarkar, Energetic and electronic structure of penta-graphene nanoribbons, Carbon 100 (2016) 118–125.

[5] J.M. de Sousa, A.L. Aguiar, E.C. Girão, A.F. Fonseca, A. Souza Filho, D.S. Galvao, Mechanical properties of pentagraphene-based nanotubes: a molecular dynamics study, MRS Adv. 3 (1–2) (2018) 97–102.

[6] Z. Wang, F. Dong, B. Shen, R. Zhang, Y. Zheng, L. Chen, S. Wang, C. Wang, K. Ho, Y.-J. Fan, Electronic and optical properties of novel carbon allotropes, Carbon 101 (2016) 77–85.

[7] Z.G. Yu, Y.-W. Zhang, A comparative density functional study on electrical properties of layered penta-graphene, J. Appl. Phys. 118 (16) (2015) 165706.

[8] X. Zhu, H. Su, Chiral pentagon only diamond-like structures, J. Phys. Chem. C 121 (25) (2017) 13810–13815.

[9] X. Li, S. Zhang, F.Q. Wang, Y. Guo, J. Liu, Q. Wang, Tuning the electronic and mechanical properties of penta-graphene via hydrogenation and fluorination, Phys. Chem. Chem. Phys. 18 (21) (2016) 14191–14197.

[10] A. Luo, R. Hu, Z. Fan, H. Zhang, J. Yuan, C. Yang, Z. Zhang, Electronic structure, carrier mobility and device properties for mixed-edge phagraphene nanoribbon by hetero-atom doping, Org. Electron. 51 (2017) 277–286.

[11] R. Krishnan, S.-Y. Wu, H.-T. Chen, Nitrogen-doped penta-graphene as a superior catalytic activity for CO oxidation, Carbon 132 (2018) 257–262.

[12] H. Qin, C. Feng, X. Luan, D. Yang, First-principles investigation of adsorption behaviors of small molecules on penta-graphene, Nanoscale Res. Lett. 13 (1) (2018) 264.

[13] R. Krishnan, S.-Y. Wu, H.-T. Chen, Catalytic CO oxidation on B-doped and BN co-doped penta-graphene: a computational study, Phys. Chem. Chem. Phys. 20 (41) (2018) 26414–26421.

[14] A. Lopez-Bezanilla, P.B. Littlewood, σ−π-Band inversion in a novel two-dimensional material, J. Phys. Chem. C 119 (33) (2015) 19469–19474.

[15] C. Zhang, S. Zhang, Q. Wang, Bonding-restricted structure search for novel 2D materials with dispersed C 2 dimers, Sci. Rep. 6 (2016) 29531.

[16] H. Liu, G. Qin, Y. Lin, M. Hu, Disparate strain dependent thermal conductivity of two-dimensional penta-structures, Nano Lett. 16 (6) (2016) 3831–3842.

[17] F. Li, K. Tu, H. Zhang, Z. Chen, Flexible structural and electronic properties of a pentagonal B 2 C monolayer via external strain: a computational investigation, Phys. Chem. Chem. Phys. 17 (37) (2015) 24151–24156.

[18] Y. Wang, Y. Li, Z. Chen, Not your familiar two dimensional transition metal disulfide: structural and electronic properties of the PdS 2 monolayer, J. Mater. Chem. C 3 (37) (2015) 9603–9608.

[19] S. Zhang, J. Zhou, Q. Wang, P. Jena, Beyond graphitic carbon nitride: nitrogen-rich penta-CN2 sheet, J. Phys. Chem. C 120 (7) (2016) 3993–3998.

[20] Y. Ding, Y. Wang, Hydrogen-induced stabilization and tunable electronic structures of penta-silicene: a computational study, J. Mater. Chem. C 3 (43) (2015) 11341–11348.

[21] L.-S. Zhao, Y. Wang, C.-P. Chen, L.-L. Liu, H.-X. Yu, Y. Zhang, Y. Chen, X.-C. Wang, Elastic, electronic and optical properties of stable pentagonal ZnO2, Phys. E Low-dimens. Syst. Nanostruct. 91 (2017) 82–87.

[22] Y. Ma, L. Kou, X. Li, Y. Dai, T. Heine, Room temperature quantum spin Hall states in two-dimensional crystals composed of pentagonal rings and their quantum wells, NPG Asia Mater. 8 (4) (2016) e264.

[23] J. Li, X. Fan, Y. Wei, H. Liu, S. Li, P. Zhao, G. Chen, Half-metallicity and ferromagnetism in penta-AlN 2 nanostructure, Sci. Rep. 6 (2016) 33060.

[24] A.D. Oyedele, S. Yang, L. Liang, A.A. Puretzky, K. Wang, J. Zhang, P. Yu, P.R. Pudasaini, A.W. Ghosh, Z. Liu, PdSe2: pentagonal two-dimensional layers with high air stability for electronics, J. Am. Chem. Soc. 139 (40) (2017) 14090–14097.

[25] H. Einollahzadeh, R. Dariani, S. Fazeli, Computing the band structure and energy gap of penta-graphene by using DFT and G0W0 approximations, Solid State Commun. 229 (2016) 1–4.

[26] T. Stauber, J. Beltrán, J. Schliemann, Tight-binding approach to penta-graphene, Sci. Rep. 6 (2016) 22672.

[27] H. Sun, S. Mukherjee, C.V. Singh, Mechanical properties of monolayer penta-graphene and phagraphene: a first-principles study, Phys. Chem. Chem. Phys. 18 (38) (2016) 26736–26742.

[28] F.Q. Wang, J. Yu, Q. Wang, Y. Kawazoe, P. Jena, Lattice thermal conductivity of penta-graphene, Carbon 105 (2016) 424–429.

[29] X. Wu, V. Varshney, J. Lee, T. Zhang, J.L. Wohlwend, A.K. Roy, T. Luo, Hydrogenation of penta-graphene leads to unexpected large improvement in thermal conductivity, Nano Lett. 16 (6) (2016) 3925–3935.

[30] F.Q. Wang, J. Liu, X. Li, Q. Wang, Y. Kawazoe, Weak interlayer dependence of lattice thermal conductivity on stacking thickness of penta-graphene, Appl. Phys. Lett. 111 (19) (2017), 192102.

[31] Y. Guo, F.Q. Wang, Q. Wang, An all-carbon vdW heterojunction composed of penta-graphene and graphene: tuning the Schottky barrier by electrostatic gating or nitrogen doping, Appl. Phys. Lett. 111 (7) (2017), 073503.

[32] W. Xu, G. Zhang, B. Li, Thermal conductivity of penta-graphene from molecular dynamics study, J. Chem. Phys. 143 (15) (2015), 154703.

[33] Y.-Y. Zhang, Q.-X. Pei, Y. Cheng, Y.-W. Zhang, X. Zhang, Thermal conductivity of penta-graphene: the role of chemical functionalization, Comput. Mater. Sci. 137 (2017) 195–200.

[34] J. Quijano-Briones, H. Fernández-Escamilla, A. Tlahuice-Flores, Chiral penta-graphene nanotubes: structure, bonding and electronic properties, Comput. Theor. Chem. 1108 (2017) 70–75.

[35] J. Quijano-Briones, H. Fernández-Escamilla, A. Tlahuice-Flores, Doped penta-graphene and hydrogenation of its related structures: a structural and electronic DFT-D study, Phys. Chem. Chem. Phys. 18 (23) (2016) 15505–15509.

[36] L.-L. Liu, Y. Wang, C.-P. Chen, H.-X. Yu, L.-S. Zhao, X.-C. Wang, Tuning the electronic and magnetic properties of penta-graphene using a hydrogen atom: a theoretical study, RSC Adv. 7 (64) (2017) 40200–40207.

[37] A.A. Balandin, Thermal properties of graphene and nanostructured carbon materials, Nat. Mater. 10 (8) (2011) 569.

[38] A.A. Balandin, S. Ghosh, W. Bao, I. Calizo, D. Teweldebrhan, F. Miao, C.N. Lau, Superior thermal conductivity of single-layer graphene, Nano Lett. 8 (3) (2008) 902–907.

[39] W. Cai, A.L. Moore, Y. Zhu, X. Li, S. Chen, L. Shi, R.S. Ruoff, Thermal transport in suspended and supported monolayer graphene grown by chemical vapor deposition, Nano Lett. 10 (5) (2010) 1645–1651.

[40] S. Ghosh, W. Bao, D.L. Nika, S. Subrina, E.P. Pokatilov, C.N. Lau, A.A. Balandin, Dimensional crossover of thermal transport in few-layer graphene, Nat. Mater. 9 (7) (2010) 555.

[41] S. Chen, A.L. Moore, W. Cai, J.W. Suk, J. An, C. Mishra, C. Amos, C.W. Magnuson, J. Kang, L. Shi, Raman measurements of thermal transport in suspended monolayer graphene of variable sizes in vacuum and gaseous environments, ACS Nano 5 (1) (2010) 321–328.

[42] D. Kotchetkov, J. Zou, A. Balandin, D. Florescu, F.H. Pollak, Effect of dislocations on thermal conductivity of GaN layers, Appl. Phys. Lett. 79 (26) (2001) 4316–4318.

[43] J. Zou, D. Kotchetkov, A. Balandin, D. Florescu, F.H. Pollak, Thermal conductivity of GaN films: effects of impurities and dislocations, J. Appl. Phys. 92 (5) (2002) 2534–2539.

[44] A.Y. Serov, Z.-Y. Ong, E. Pop, Effect of grain boundaries on thermal transport in graphene, Appl. Phys. Lett. 102 (3) (2013), 033104.

[45] Z.G. Fthenakis, Z. Zhu, D. Tománek, Effect of structural defects on the thermal conductivity of graphene: from point to line defects to haeckelites, Phys. Rev. B 89 (12) (2014) 125421.

[46] K. Azizi, P. Hirvonen, Z. Fan, A. Harju, K.R. Elder, T. Ala-Nissila, S.M.V. Allaei, Kapitza thermal resistance across individual grain boundaries in graphene, Carbon 125 (2017) 384–390.

[47] P. Schelling, S. Phillpot, P. Keblinski, Kapitza conductance and phonon scattering at grain boundaries by simulation, J. Appl. Phys. 95 (11) (2004) 6082–6091.

[48] K.R. Hahn, C. Melis, L. Colombo, Thermal transport in nanocrystalline graphene investigated by approach-to-equilibrium molecular dynamics simulations, Carbon 96 (2016) 429–438.

[49] T. Ma, Z. Liu, J. Wen, Y. Gao, X. Ren, H. Chen, C. Jin, X.-L. Ma, N. Xu, H.-M. Cheng, Tailoring the thermal and electrical transport properties of graphene films by grain size engineering, Nat. Commun. 8 (2017) 14486.

[50] A. Bagri, S.-P. Kim, R.S. Ruoff, V.B. Shenoy, Thermal transport across twin grain boundaries in polycrystalline graphene from nonequilibrium molecular dynamics simulations, Nano Lett. 11 (9) (2011) 3917–3921.

[51] F. Müller-Plathe, A simple nonequilibrium molecular dynamics method for calculating the thermal conductivity, J. Chem. Phys. 106 (14) (1997) 6082–6085.

[52] P. Delhaes, Graphite and Precursors, CRC Press, 2014.

[53] C. Oligschleger, J. Schön, Simulation of thermal conductivity and heat transport in solids, Phys. Rev. B 59 (6) (1999) 4125.

[54] R.H. Poetzsch, H. Böttger, Interplay of disorder and anharmonicity in heat conduction: molecular-dynamics study, Phys. Rev. B 50 (21) (1994) 15757.

[55] S. Winczewski, M.Y. Shaheen, J. Rybicki, Interatomic potential suitable for the modeling of penta-graphene: molecular statics/molecular dynamics studies, Carbon 126 (2018) 165–175.

[56] P. Erhart, K. Albe, Analytical potential for atomistic simulations of silicon, carbon, and silicon carbide, Phys. Rev. B 71 (3) (2005), 035211.

[57] R. Grantab, V.B. Shenoy, R.S. Ruoff, Anomalous strength characteristics of tilt grain boundaries in graphene, Science 330 (6006) (2010) 946–948.

[58] P.Y. Huang, C.S. Ruiz-Vargas, A.M. van der Zande, W.S. Whitney, M.P. Levendorf, J.W. Kevek, S. Garg, J.S. Alden, C.J. Hustedt, Y. Zhu, Grains and grain boundaries in single-layer graphene atomic patchwork quilts, Nature 469 (7330) (2011) 389.

[59] Q. Yu, L.A. Jauregui, W. Wu, R. Colby, J. Tian, Z. Su, H. Cao, Z. Liu, D. Pandey, D. Wei, Control and characterization of individual grains and grain boundaries in graphene grown by chemical vapour deposition, Nat. Mater. 10 (6) (2011) 443.

[60] D.L. Duong, G.H. Han, S.M. Lee, F. Gunes, E.S. Kim, S.T. Kim, H. Kim, Q.H. Ta, K.P. So, S.J. Yoon, Probing graphene grain boundaries with optical microscopy, Nature 490 (7419) (2012) 235.

[61] H. Ogawa, GBstudio: a builder software on periodic models of CSL boundaries for molecular simulation, Mater. Trans. 47 (11) (2006) 2706–2710.

[62] A. Togo, F. Oba, I. Tanaka, First-principles calculations of the ferroelastic transition between rutile-type and CaCl 2-type SiO 2 at high pressures, Phys. Rev. B 78 (13) (2008) 134106.

[63] C. Ren, W. Zhang, Z. Xu, Z. Zhu, P. Huai, Thermal conductivity of single-walled carbon nanotubes under axial stress, J. Phys. Chem. C 114 (13) (2010) 5786–5791.

[64] M. Hu, Y. Jing, X. Zhang, Low thermal conductivity of graphene nanotubes from molecular dynamics study, Phys. Rev. B 91 (15) (2015), 155408.

[65] M.A. Angadi, T. Watanabe, A. Bodapati, X. Xiao, O. Auciello, J.A. Carlisle, J.A. Eastman, P. Keblinski, P.K. Schelling, S.R. Phillpot, Thermal transport and grain boundary conductance in ultrananocrystalline diamond thin films, J. Appl. Phys. 99 (11) (2006), 114301.

[66] V. Samvedi, V. Tomar, The role of interface thermal boundary resistance in the overall thermal conductivity of Si–Ge multilayered structures, Nanotechnology 20 (36) (2009), 365701.

[67] A. Maiti, G. Mahan, S. Pantelides, Dynamical simulations of nonequilibrium processes—heat flow and the Kapitza resistance across grain boundaries, Solid State Commun. 102 (7) (1997) 517–521.

[68] P.K. Schelling, S.R. Phillpot, P. Keblinski, Comparison of atomic-level simulation methods for computing thermal conductivity, Phys. Rev. B 65 (14) (2002), 144306.